Angewandte Chemie
Eine Zeitschrift der Gesellschaft Deutscher Chemiker

Supporting Information

Formation of LiF-rich Cathode-Electrolyte Interphase by Electrolyte Reduction

P. Bai, X. Ji, J. Zhang, W. Zhang, S. Hou, H. Su, M. Li, T. Deng, L. Cao, S. Liu, X. He, Y. Xu, C. Wang**

Author Contributions

C.W. Conceptualization:Supporting; Supervision:Equal; Writing – review & editing:Equal
P.B. Conceptualization:Lead; Data curation:Lead; Formal analysis:Lead; Writing – original draft:Lead
X.J. Conceptualization:Supporting; Formal analysis:Supporting
j.Z. Formal analysis:Supporting; Resources:Supporting
W.Z. Formal analysis:Supporting; Resources:Supporting
S.H. Formal analysis:Supporting; Methodology:Supporting
H.S. Formal analysis:Supporting; Resources:Supporting
M.L. Formal analysis:Supporting; Resources:Supporting
T.D. Methodology:Supporting; Software:Supporting
L.C. Methodology:Supporting; Resources:Supporting
S.L. Methodology:Supporting; Software:Supporting
X.H. Resources:Supporting; Software:Supporting
Y.X. Conceptualization:Supporting; Supervision:Equal; Writing – review & editing:Equal

Supporting Information

69451 Weinheim, Germany

Formation of LiF-rich Cathode-Electrolyte Interphase by Electrolyte Reduction

Panxing Bai[a] [b], Xiao Ji[a], Jiaxun Zhang[a], Weiran Zhang[a], Singyuk Hou[a], Hai Su[b], Mengjie Li[b], Tao Deng[a], Longsheng Cao[a], Sufu Liu[a], Xinzi He[a], Yunhua Xu*[b], and Chunsheng Wang*[a]

Abstract: The capacity of transition metal oxide cathode for Li-ion batteries can be further enhanced by increasing the charging potential. However, these high voltage cathodes suffer from fast capacity decay because the large volume change of cathode breaks the active materials and cathode electrolyte interphase (CEI), resulting in electrolyte penetration into broken active materials and continuous side reactions between cathode and electrolytes. Herein, a robust LiF-rich CEI was formed by potentiostatic reduction of fluorinated electrolyte at a low potential of 1.7 V. By taking $LiCoO_2$ as a model cathode, we demonstrate that the LiF-rich CEI maintains the structural integrity and suppresses electrolyte penetration at a high cut-off potential of 4.6 V. The $LiCoO_2$ with LiF-rich CEI exhibited a capacity of 198 mAh g-1 at 0.5C and an enhanced capacity retention of 63.5% over 400 cycles as compared to the LiF-free $LiCoO_2$ with only 17.4% of capacity retention.

SUPPORTING INFORMATION

Experimental section

***Electrolyte and Electrode Preparation**:* Fuoroethylene carbonate (FEC, 99.9%, Gotion), diethyl carbonate (DEC, 99%, Sigma-Aldrich) and ethylene carbonate (EC, 99%, Sigma-Aldrich) were dried overnight by molecular sieves (4 Å, Sigma-Aldrich) before preparing the electrolytes to make sure the water content is lower than 10 ppm, which was tested using a Karl-Fischer titration (Metrohm 899 Coulometer). Lithium difluoro(oxalato)borate (LiDFOB, 99.9%), lithium tetrafluoroborate ($LiBF_4$, 99.99%) and lithium tetrafluoroborate ($LiPF_6$, 99.99%) were purchased from Sigma-Aldrich and used as received. A dual-salt 1M LiDFOB and 0.2 M $LiBF_4$ (FEC: DEC, 1:2 volume ratio) electrolyte and other comparisons were all prepared in an Ar-filled glovebox (M-Braun) with the moisture and oxygen contents less than 0.5 ppm. All used $LiCoO_2$ (LCO), graphite and lithium titanium oxide (LTO) electrodes were kindly provided by Saft America Inc. The areal capacity of $LiCoO_2$ and LTO is 1.5 mAh cm^{-2} for half-cells. For $LiCoO_2$//graphite full cells, the areal capacity of $LiCoO_2$ and graphite are 3 mAh cm^{-2}. The LCO and LTO electrodes were pouched into 9 mm diameter while 9.52 mm (3/8 inch) for graphite. All the electrodes were vacuum dried overnight at 100 ℃ and then transferred to an Ar filled glovebox.

***Electrochemical measurements**:* In an argon-filled glovebox (O_2 < 0.5 ppm, H_2O < 0.5 ppm), CR2032 coin-type half-cells were assembled by sandwiching one piece of polyethylene separator (Celgard, sigma-Aldrich) and one piece of glass fiber (GF/A, sigma-Aldrich) between the LCO/Graphite/or LTO electrodes and Li chips with a thickness of 550 μm (China Energy Lithium Company). In the normal galvanostatic cell tests, the LCO//Li coin cells were loaded into a battery tester (Neware instruments) and cycled between 2.8 and 4.6 V. For the pre-potentiostatic ones, LCO//Li coin cells were firstly discharged to 1.7 V or other voltages (2.0, 1.4 and 1.0 V) (vs. Li^+/Li) and held for different period lengths, including 24 and 120 h, during which electrolyte reduction occurred. For the external electrical shorting, LCO//Li coin cells were clamped by conducting metal tweezer to become shorted for 10 or 20 s. Then the cells were cycled between 2.8 and 4.6 V. To form better CEI, repeat the 1.7 V potentiostatic step during initial five cycles within 1.7-4.6 V and then normally charge/discharge the cells within voltage range of 2.8-4.6 V (vs. Li^+/Li). The graphite//Li coin cells were tested in a voltage range of 0.01-2.00 V (vs. Li^+/Li). For LCO//Graphite full-cell configuration, cells were cycled at 0.5C (calculated based on LCO cathode) in the potential window of 2.80-4.55 V, where fresh LCO or potentiostatic processed LCO were used. The N/P is 1.03. The separator still contains one piece of polyethylene and one piece of glass fiber. Three-electrode coin cell using a small piece of lithium metal as a reference electrode between lithiated LTO (discharge LTO//Li cell to the plateau with a capacity of 0.5 mAh cm^{-2}) and fresh LCO was configured to individually monitor the potential of LCO vs Li^+/Li by Arbin battery test station (BT2000, Arbin Instruments). To test the practical application, the lithiated LTO//LCO cell was discharged to 0 V and held to achieve the potentiostatic process. The treated LCO electrodes were extracted and matched with graphite anodes. All the electrochemical measurements were conducted at about 25 ℃.

The reduction and oxidation stability of the electrolyte in Li//stainless-steel or LCO//Li cells with or without potentiostatic steps were evaluated by linear sweep voltammetry (LSV) on a Gamry 1000E electrochemical workstation (USA). The electrochemical floating test was performed using LCO//Li half-cell configuration. The cells with or without potentiostatic steps were charged to 4.6 V at 0.5C and then maintained for 180 h with the current being monitored by Arbin battery test station. Electrochemical impedance spectroscopy (EIS) measurements were conducted on a Gamry 1000E electrochemical workstation (USA). Impedance spectra were collected from the LCO//Li cells in the fully charged state over a frequency range from 10^6 to 0.01 Hz by applying a 10-mV potential amplitude.

***Characterizations**:* For postmortem analysis, including X-ray diffraction (XRD), scanning electron microscopy (SEM), transmission electron microscopy (TEM), X-ray photoelectron spectroscopy (XPS) and time-of-flight secondary ion mass spectrometry (TOF-SIMS) measurements, the cycled cells were carefully disassembled inside the glovebox, and the recovered electrodes were thoroughly washed with anhydrous DEC three times to remove any residual salt and electrolyte, and then dried under vacuum overnight before testing. The phases and crystallographic structures were investigated by XRD patterns on a D8 Advance with LynxEye and SolX (Bruker AXS, USA) using Cu Kα radiation (λ=1.5418 Å). To avoid the influence of air and moisture during the test, the dried samples in glovebox were sealed on the holder with adhesive tape. The morphologies were characterized using a Hitachi SU-70 field emission SEM equipped with an energy-dispersive X-ray spectroscopy detector and a JEOL 2100F field emission TEM equipped with a Gatan Oneview camera operated at 200 kV. To examine the internal structure, cross-sections were carried out on a Ga^+ focused ion beam (FIB)/SEM (Tescan GAIA3) at an accelerated voltage of 30 kV and 48 pA current. All SEM and TEM sample preparations were conducted in glovebox, transferred into an Ar-filled bag, and then briefly exposed to air for less than 30 s when loading into the instruments. The surface or in-depth chemistry of LCO was examined directly or after Ar^+ ion sputtering by XPS on a high sensitivity Kratos Axis 165 X-ray photoelectron spectrometer with a Mg Kα radiation. The binding energy of all peaks were calibrated to the C-C peak at 284.8 eV. CasaXPS was used for data analysis, using Shirley-type backgrounds and Gaussian-Lorentzian (30) peak shapes to fit. Quantification was done with relative sensitivity factors (RSF) from the Kratos vision library. The sample holder was transferred from glovebox to the XPS chamber under argon protection to avoid any contamination by air or moisture. The in-depth spatial distribution of the constituent elements was analyzed via TOF-SIMs attached to a Ga^+ FIB/SEM (Tescan GAIA3) at an accelerated voltage of 30 kV and a current of 48 pA. The amount of dissolved Co ions was measured through inductively coupled plasma atomic emission spectrometer (ICP-AES) determined by an an ICPE-9000 (ICP Atomic Emission Spectrometer).

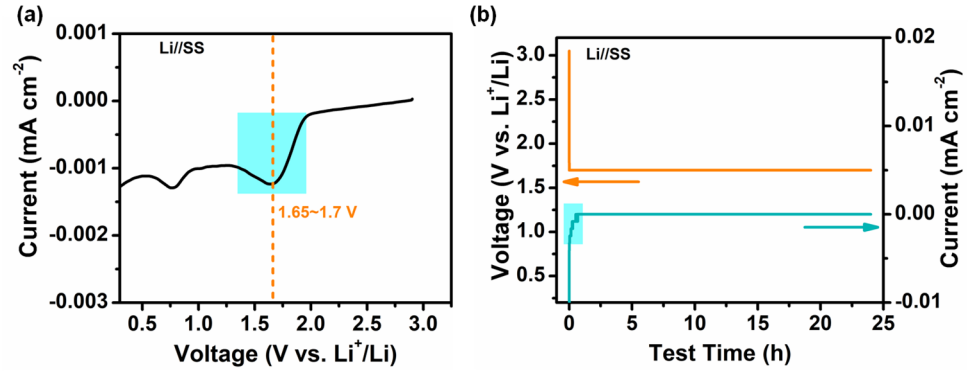

Figure S1. Reductive electrochemistry and potentiostatic experiment results with LiDFOB-$LiBF_4$ electrolyte as evaluated on stainless steel (SS) electrodes. a) LSV curve at a scanning rate of 0.1 mV s^{-1}. b) Evolution of the current with voltage hold at 1.7 V.

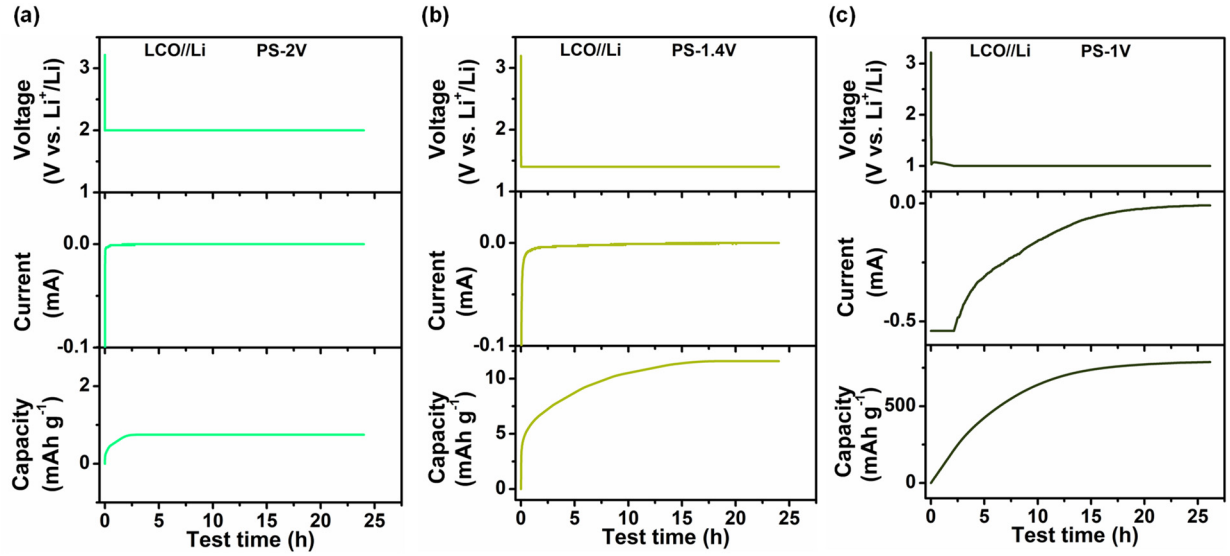

Figure S2. Current and capacity response in LCO//Li cells subjected to the first discharge and potentiostatic with voltage hold at a) 2.0 V, b) 1.4 V and c) 1.0 V for 24 h.

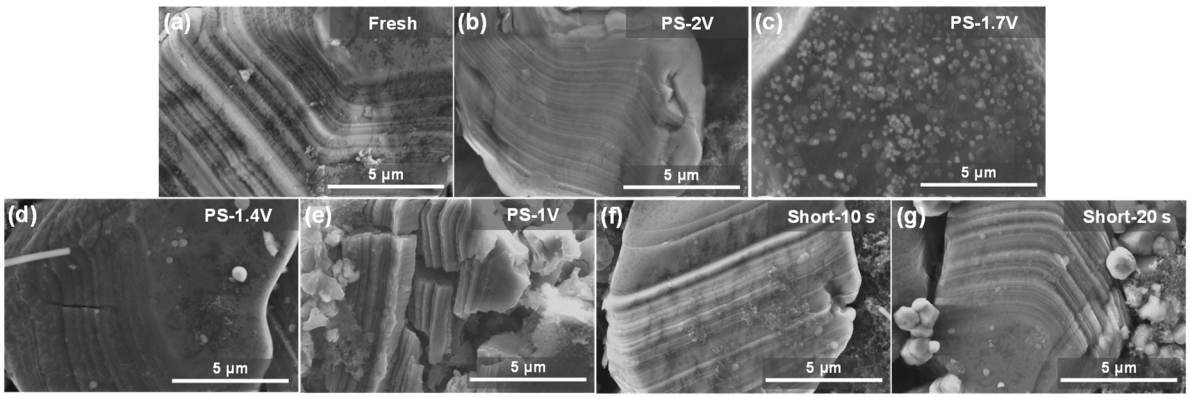

Figure S3. SEM characterization for the LCO electrodes under different potentiostatic and electrical shorting conditions. a) pristine (fresh). With voltage holding at b) 2.0 V, c) 1.7 V, d) 1.4 V and e) 1.0 V for 24 h, as well as upon external electrical shorting for f) 10 s and g) 20 s.

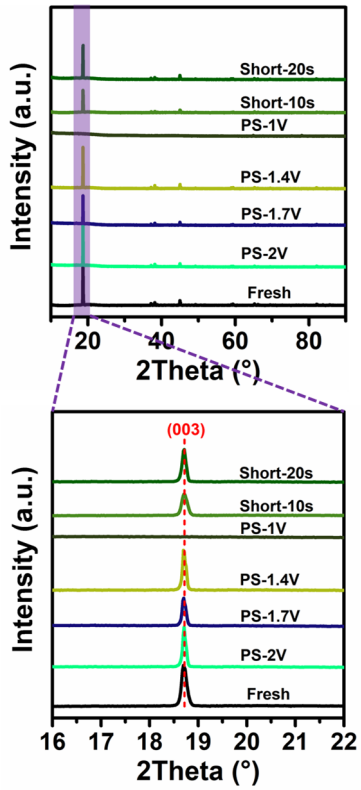

Figure S4. Ex-situ XRD characterization for the LCO electrodes after different potentiostatic and electrical shorting conditions.

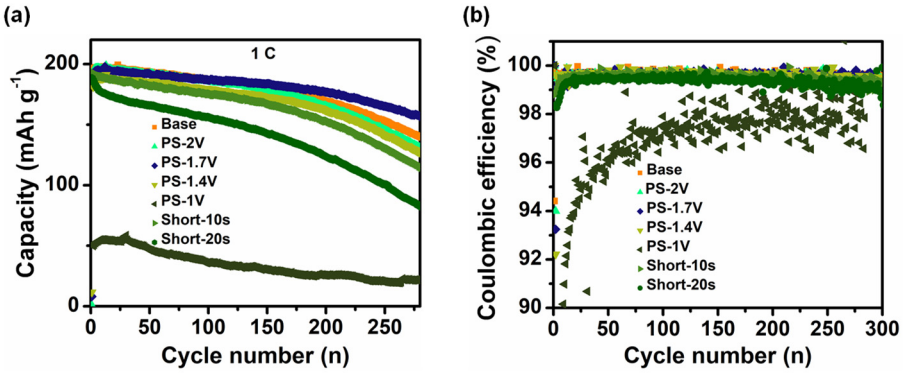

Figure S5. Galvanostatic cycling comparison of LCO//Li with different potentiostatic and electrical shorting conditions. The current rate is 1C.

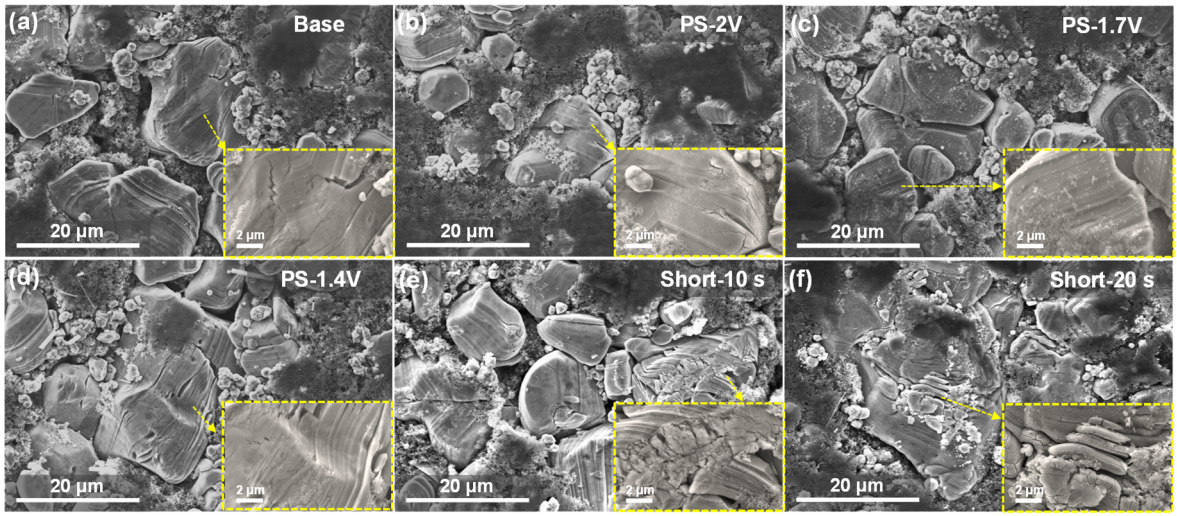

Figure S6. SEM characterization for the cycled LCO electrodes (280 cycles) with different potentiostatic and electrical shorting conditions. a) Base and with voltage holding at b) 2.0 V, c) 1.7 V and d) 1.4 V for 24 h, as well as upon external electrical shorting for e) 10 s and f) 20 s. The insets show the enlarged view regions.

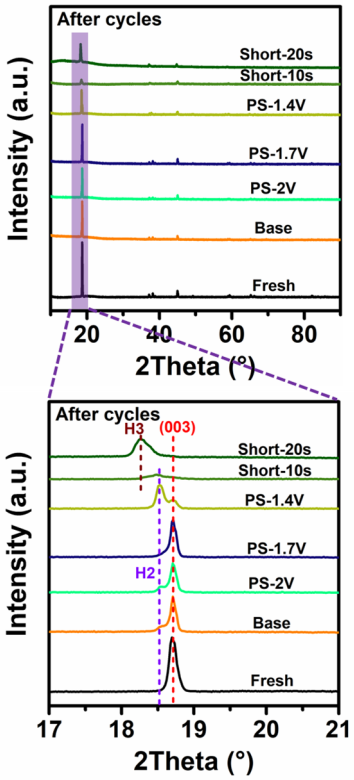

Figure S7. The ex-situ XRD characterization for the cycled LCO electrodes (280 cycles) with different potentiostatic and electrical shorting conditions.

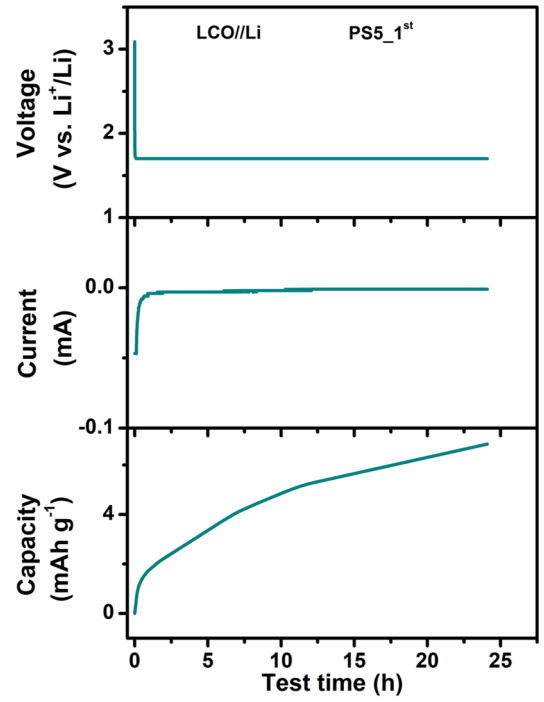

Figure S8. Current and capacity response of PS5 during first discharge and potentiostatic step.

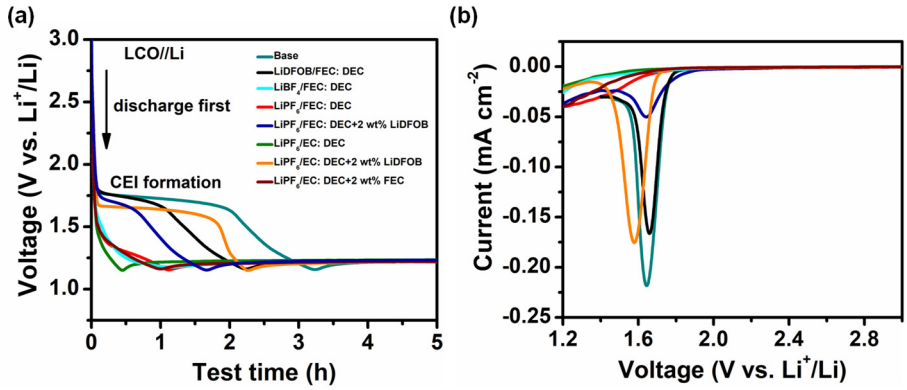

Figure S9. Reductive electrochemistry of different electrolytes with/or without LiDFOB or FEC species evaluated on LCO//Li cells. a) Voltage profiles for the initial discharge at a current rate of 2 mA g^{-1}. b) LSV curves scanned to 1.2 V at 0.1 mV s^{-1}.

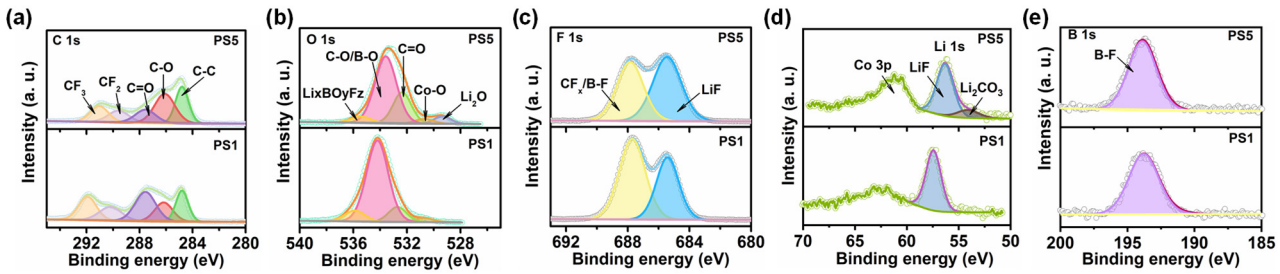

Figure S10. Comparison of the CEI components formed on LCO in PS1 and PS5 by comparative XPS spectra of a) C 1s, b) O 1s, c) F 1s, d) Li 1s, and e) B 1s.

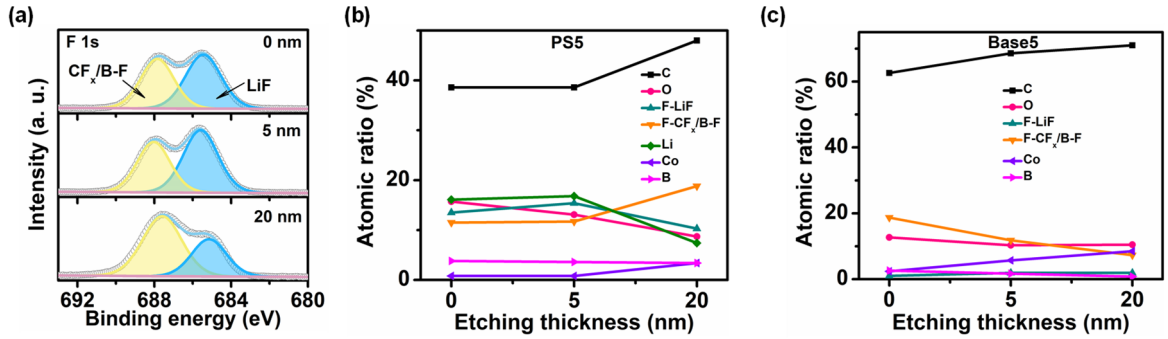

Figure S11. In-depth XPS results with etching thickness of 5 and 20 nm for formed CEI. a) Typical spectra of F 1s recorded in PS5. Depth profiles of the atomic concentration of C, O, F and B elements in b) PS5 and c) Base5.

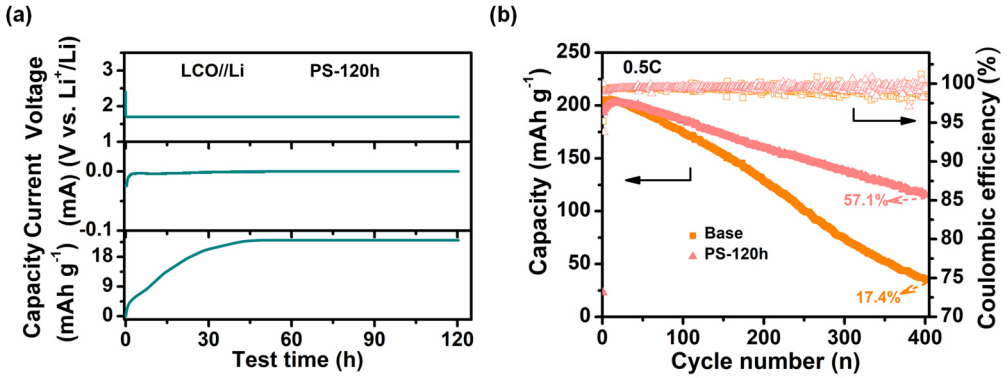

Figure S12. LiF-rich CEI formed on LCO via potentiostatic step at 1.7 V for 120 h and its improvement on long-term cycling stability.

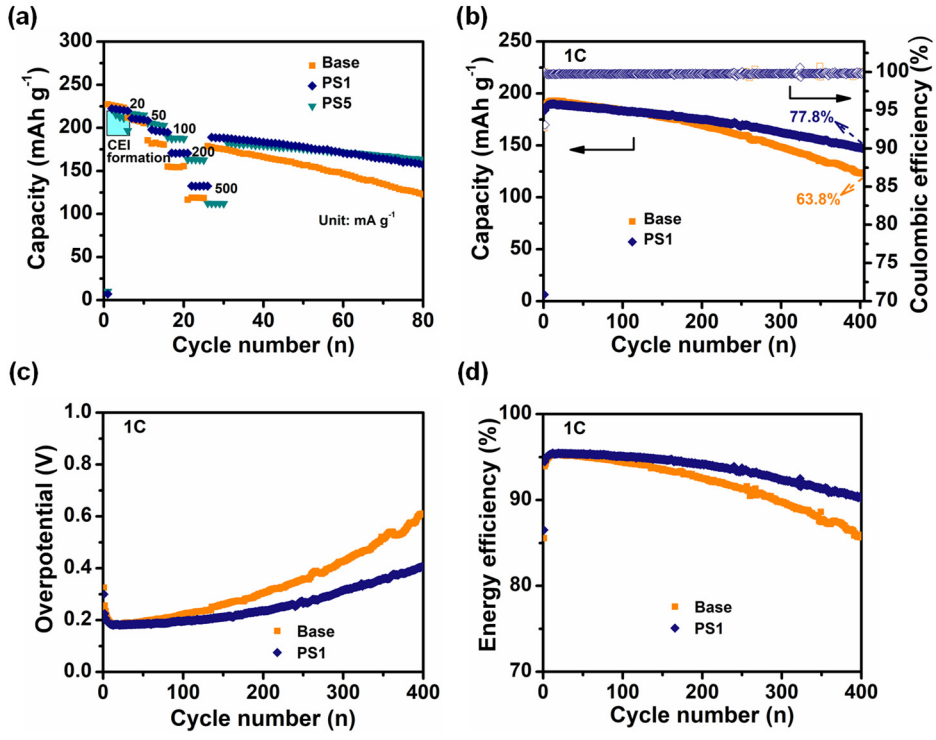

Figure S13. a) Rate performance comparison of LCO//Li cells with/or without LiF-rich CEI. Comparison of b) long-term cycling stability, c) overpotentials and d) energy efficiency under 1C. Note that, the number of cycles in PS1 towards overpotentials and energy efficiency was calculated after deducting the initial potentiostatic cycle. All cells were tested at a constant temperature of 25 ℃ within the 2.8-4.6 V except for the initial potentiostatic step.

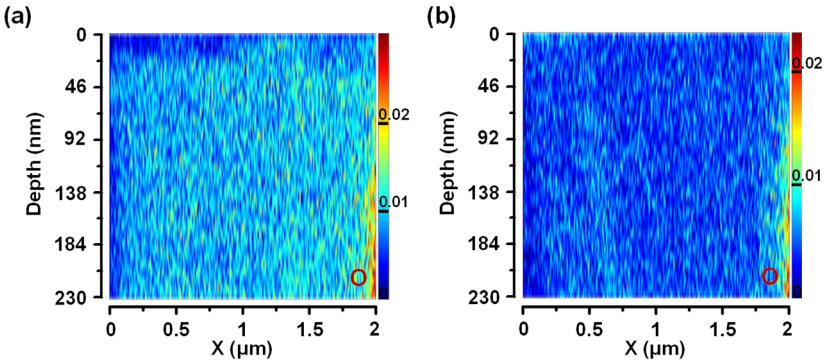

Figure S14. Corresponding spatial O mapping on cycled LCO electrodes in a) PS5 and b) Base as indicated by TOF-SIMS.

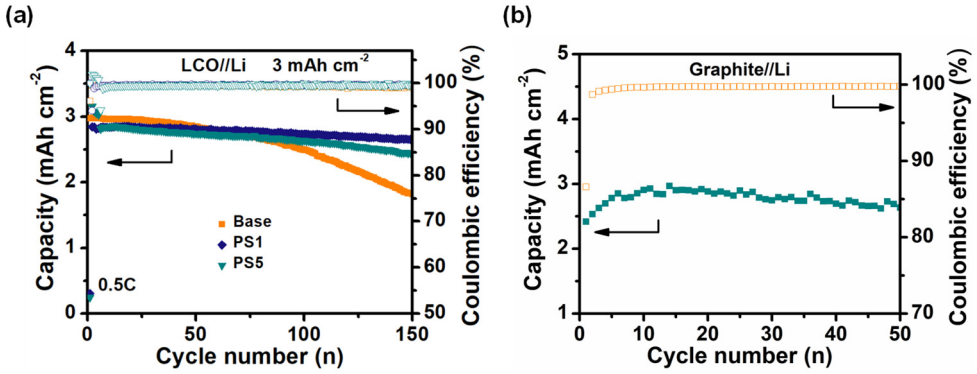

Figure S15. Electrochemical evaluation of higher-capacity LCO (3 mAh cm^{-2}) and graphite electrodes for full-cell configuration. a) Cycling stability comparison of LCO//Li cells in Base, PS1 and PS5 at a current rate of 0.5C. b) Cycling performance of graphite//Li cells at the same current.

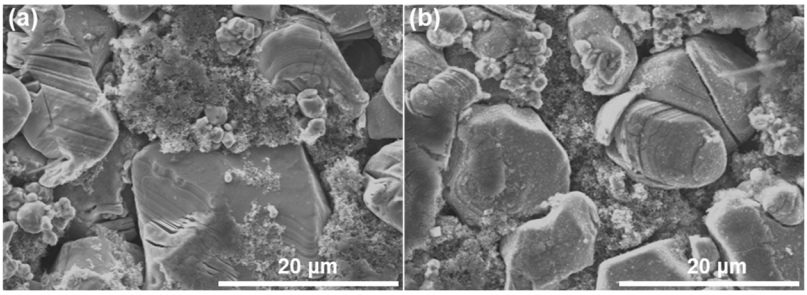

Figure S16. SEM characterization of LCO electrodes extracted from full cells of a) base LCO//Graphite and b) LiF-rich CEI protected LCO//Graphite after 500 cycles. The insets show the enlarged view regions.

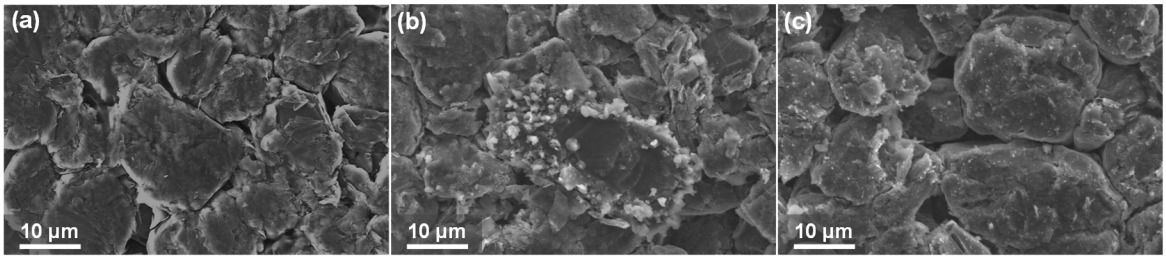

Figure S17. SEM characterization of a) pristine graphite electrodes, and the ones extracted from full cells of b) base LCO//Graphite and c) LiF-rich CEI protected LCO//Graphite after 500 cycles.

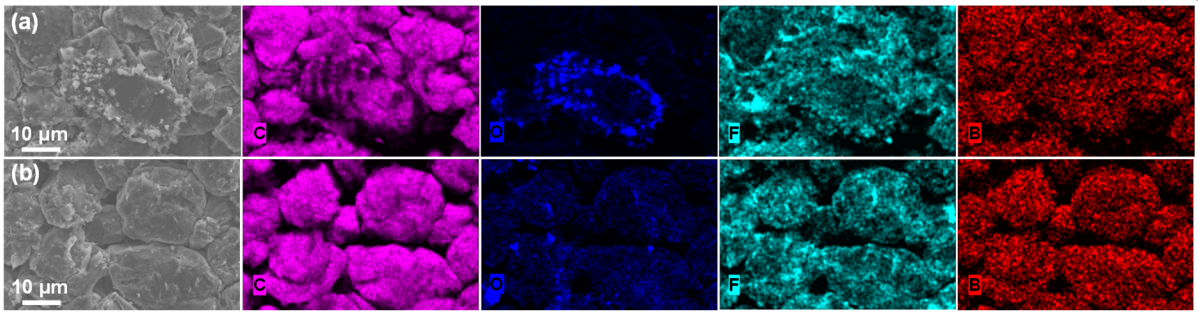

Figure S18. SEM images and corresponding elemental mapping of graphite electrodes extracted from full cells of a) base LCO//Graphite and b) LiF-rich CEI protected LCO//Graphite after 500 cycles.

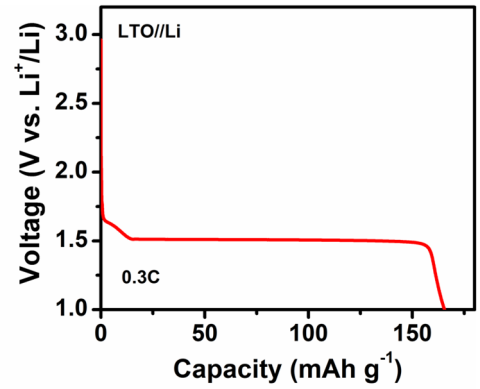

Figure S19. Galvanostatic discharge profile of LTO//Li cell at 0.3C.

SUPPORTING INFORMATION

Table S1. Comparison of electrochemical properties of the reported LCO-based LIBs cycled at cut-off voltage of 4.5 V and 4.6 V with different modified methods, including coating, doping and electrolyte/interface/binder optimizations.

Method	Cell configuration	Cut-off voltage (V)	Areal loading (mg cm^{-2})	Current density (mA g^{-1})	Capacity retention (%) at (cycle number)	Ref.
Predischarge and potentiostatic reduction	LCO//Li	4.6	7.4	100	63.5 (400) 73.1 (300) 83 (200) 93.2 (100)	This work
Predischarge and potentiostatic reduction	LCO//Li	4.6	7.4	200	77.8 (400) 85.5 (300) 92.2 (200) 96.5 (100)	This work
Predischarge and potentiostatic reduction	LCO//Graphite	4.55	14.8	100	85 (500) 88.8 (400) 91.8 (300) 94 (200) 95.6 (100)	This work
TMB-added eelctrolyte	LCO//Graphite	4.5	_	57	66 (200)	[1]
Li-Al-F-modified LCO	LCO//Li LCO//Graphite	4.6 4.6	12.6±0.3 12.6±0.3	27.4 27.4	81.8 (200) 78.4 (70)	[2]
La and Al-doping LCO	LCO//Li	4.5	_	_	96 (50)	[3]
Ti-Mg-Al doping LCO	LCO//Li	4.6	3.0-4.0	137	86 (100)	[4]
Al-Ti-Mg doping LCO	LCO//Li LCO//MCMB	4.6 4.5	1.5±0.2 7.0±0.2	70 70	78 (200) 78 (200)	[5]
PDTD-added electrolyte	LCO//Li LCO//Graphite	4.6 4.45	_	_	57 (150) 68 (150)	[6]
DMC/HFE/FEC/MSM electrolyte	LCO//Li	4.55	12.4	200	75 (300)	[7]
LiFSI-DME-TTE	LCO//Li	4.5	13.5	Charge: 46 Discharge: 141	80 (800)	[8]
F-HTCN additive in electrolyte	LCO//Li	4.6	6.0	200	75 (300)	[9]
Se-substituted LCO	LCO//Li LCO//Graphite	4.62 4.57	16.0-17.0 16.0-17.0	70 100	87 (120) 80 (450)	[10]
LATP and Li_3PO_4-coated LCO	LCO//Li	4.6	3.0	137	88.3 (100)	[11]
FEC-DMC-HFE electrolyte	LCO//Li	4.5	8.0	200	84 (300)	[12]
LMNO-coated LCO	LCO//Li LCO//Graphite	4.6 4.55	17.0 17.0	50 100	80 (100) 81.6 (300)	[13]
LiTFSI-LiDFOB-SN electrolyte	LCO//Li LCO//Graphite	4.7 4.45	34.5 34.5	274 110	70 (500) 80 (100)	[14]
AlZnO-LCO	LCO//Li	4.6	_	185	65.7 (500)	[15]
Mn-La-doping and Ti-coating LCO	LCO//Li	4.5	12.0	68.4	82.6 (300)	[16]
AIP-induced EC polymerization	LCO//Li	4.6	5.0	100	78.1 (200)	[17]
LAGP-AZO coated LCO	LCO//Li	4.6	2.0	185	77.1 (350)	[18]
Composite oxide coating LCO	LCO//Li	4.6	6.1	274	88.8 (100)	[19]
MgF_2-doping LCO	LCO//Li	4.6	3.0	270	92 (100)	[20]

LAP-coated LCO	LCO//Li LCO//Graphite	4.6 4.5	3-4 5.0	137 82.2	88.6 (200) 90.1 (90)	[21]
Ni-Ti-Mg doping LCO	LCO//Li	4.5	1.8±0.2	175	90 (100)	[22]
Mg-Pillared LCO	LCO//Li	4.6	3.0	135	84 (100)	[23]
DSL binder	LCO//Li LCO//Graphite	4.6 4.5	3.0 5.0	137 137	93.4 (100) 85.4 (100)	[24]
Sulfonamide-based electrolyte	LCO//Li	4.6	13.0	150	89 (200)	[25]
ATCN electrolyte	LCO//Li	4.5	2.3-2.6	180	91 (200)	[26]
AFTB with single-crystalline LCO	LCO//Li LCO//Graphite	4.6 4.5	7.4 18.0	137	74.8 (300) 80 (500)	[27]
$LiAlH_4$-coated LCO	LCO//Li	4.6	6.0	190	71.6 (500)	[28]
Mg doped and Se coated LCO	LCO//Li	4.6	3.0	200	90.3 (200) 72.9 (1000)	[29]

References

[1] X. Wang, L. Xing, X. Liao, X. Chen, W. Huang, Q. Yu, M. Xu, Q. Huang, W. Li, *Electrochim. Acta* **2015**, *173*, 804-811.
[2] J. Qian, L. Liu, J. Yang, S. Li, X. Wang, H. L. Zhuang, Y. Lu, *Nat. Commun.* **2018**, *9*, 4918.
[3] Q. Liu, X. Su, D. Lei, Y. Qin, J. Wen, F. Guo, Y. A. Wu, Y. Rong, R. Kou, X. Xiao, F. Aguesse, J. Bareño, Y. Ren, W. Lu, Y. Li, *Nat. Energy* **2018**, *3*, 936-943.
[4] J.-N. Zhang, Q. Li, C. Ouyang, X. Yu, M. Ge, X. Huang, E. Hu, C. Ma, S. Li, R. Xiao, W. Yang, Y. Chu, Y. Liu, H. Yu, X.-Q. Yang, X. Huang, L. Chen, H. Li, *Nat. Energy* **2019**, *4*, 594-603.
[5] L. Wang, J. Ma, C. Wang, X. Yu, R. Liu, F. Jiang, X. Sun, A. Du, X. Zhou, G. Cui, *Adv. Sci.* **2019**, *6*, 1900355.
[6] S. Wu, Y. Lin, L. Xing, G. Sun, H. Zhou, K. Xu, W. Fan, L. Yu, W. Li, *ACS Appl. Mater. Interfaces* **2019**, *11*, 17940-17951.
[7] X. Kong, R. Zhou, J. Wang, J. Zhao, *ACS Appl. Energy Mater.* **2019**, *2*, 4683-4691.
[8] X. Ren, X. Zhang, Z. Shadike, L. Zou, H. Jia, X. Cao, M. H. Engelhard, B. E. Matthews, C. Wang, B. W. Arey, X. Q. Yang, J. Liu, J. G. Zhang, W. Xu, *Adv. Mater.* **2020**, *32*, 2004898.
[9] X. Yang, M. Lin, G. Zheng, J. Wu, X. Wang, F. Ren, W. Zhang, Y. Liao, W. Zhao, Z. Zhang, N. Xu, W. Yang, Y. Yang, *Adv. Funct. Mater.* **2020**, *30*, 2004664.
[10] Z. Zhu, H. Wang, Y. Li, R. Gao, X. Xiao, Q. Yu, C. Wang, I. Waluyo, J. Ding, A. Hunt, J. Li, *Adv Mater* **2020**, *32*, 2005182.
[11] Y. Wang, Q. Zhang, Z. C. Xue, L. Yang, J. Wang, F. Meng, Q. Li, H. Pan, J. N. Zhang, Z. Jiang, W. Yang, X. Yu, L. Gu, H. Li, *Adv. Energy Mater.* **2020**, *10*, 2001413.
[12] S. Lin, J. Zhao, *ACS Appl. Mater. Interfaces* **2020**, *12*, 8316-8323.
[13] Z. Zhu, D. Yu, Z. Shi, R. Gao, X. Xiao, I. Waluyo, M. Ge, Y. Dong, W. Xue, G. Xu, W.-K. Lee, A. Hunt, J. Li, *Energy Environ. Sci.* **2020**, *13*, 1865-1878.
[14] Z. Hu, F. Xian, Z. Guo, C. Lu, X. Du, X. Cheng, S. Zhang, S. Dong, G. Cui, L. Chen, *Chem. Mater.* **2020**, *32*, 3405-3413.
[15] T. Cheng, Z. Ma, R. Qian, Y. Wang, Q. Cheng, Y. Lyu, A. Nie, B. Guo, *Adv. Funct. Mater.* **2020**, *31*, 2001974.
[16] T. Tian, T. W. Zhang, Y. C. Yin, Y. H. Tan, Y. H. Song, L. L. Lu, H. B. Yao, *Nano Lett* **2020**, *20*, 677-685.
[17] J. Yang, X. Liu, Y. Wang, X. Zhou, L. Weng, Y. Liu, Y. Ren, C. Zhao, M. Dahbi, J. Alami, D. A. Ei‐Hady, G. L. Xu, K. Amine, M. Shao, *Adv. Energy Mater.* **2021**, *11*, 2101956.
[18] T. Cheng, Q. Cheng, Y. He, M. Ge, Z. Feng, P. Li, Y. Huang, J. Zheng, Y. Lyu, B. Guo, *ACS Appl. Mater. Interfaces* **2021**, *13*, 42917-42926.
[19] A. Yano, N. Taguchi, H. Kanzaki, M. Shikano, H. Sakaebe, *J. Electrochem. Soc.* **2021**, *168*, 050517.
[20] W. Kong, J. Zhang, D. Wong, W. Yang, J. Yang, C. Schulz, X. Liu, *Angew. Chem.* **2021**, *60*, 27102-27112.
[21] X. Wang, Q. Wu, S. Li, Z. Tong, D. Wang, H. L. Zhuang, X. Wang, Y. Lu, *Energy Storage Mater.* **2021**, *37*, 67-76.
[22] S. Song, Y. Li, K. Yang, Z. Chen, J. Liu, R. Qi, Z. Li, C. Zuo, W. Zhao, N. Yang, M. Zhang, F. Pan, *J. Mater. Chem. A* **2021**, *9*, 5702-5710.
[23] Y. Huang, Y. Zhu, H. Fu, M. Ou, C. Hu, S. Yu, Z. Hu, C. T. Chen, G. Jiang, H. Gu, H. Lin, W. Luo, Y. Huang, *Angew.Chem. Int.Ed.* **2021**, *60*, 4682-4688.
[24] H. Huang, Z. Li, S. Gu, J. Bian, Y. Li, J. Chen, K. Liao, Q. Gan, Y. Wang, S. Wu, Z. Wang, W. Luo, R. Hao, Z. Wang, G. Wang, Z. Lu, *Adv. Energy Mater.* **2021**, *11*, 2101864.
[25] W. Xue, R. Gao, Z. Shi, X. Xiao, W. Zhang, Y. Zhang, Y. G. Zhu, I. Waluyo, Y. Li, M. R. Hill, Z. Zhu, S. Li, O. Kuznetsov, Y. Zhang, W.-K. Lee, A. Hunt, A. Harutyunyan, Y. Shao-Horn, J. A. Johnson, J. Li, *Energy Environ. Sci.* **2021**, *14*, 6030-6040.
[26] D. Ruan, M. Chen, X. Wen, S. Li, X. Zhou, Y. Che, J. Chen, W. Xiang, S. Li, H. Wang, X. Liu, W. Li, *Nano Energy* **2021**, *90*, 106535.
[27] J. Zhang, P. F. Wang, P. Bai, H. Wan, S. Liu, S. Hou, X. Pu, J. Xia, W. Zhang, Z. Wang, B. Nan, X. Zhang, J. Xu, C. Wang, *Adv. Mater.* **2022**, *34*, 2108353.
[28] P. Wang, Y. Meng, Y. Wang, L. Chen, Z. Zhang, W. Pu, J. Li, C. Yang, D. Xiao, *Energy Storage Mater.* **2022**, *44*, 487-496.
[29] A. Fu, Z. Zhang, J. Lin, Y. Zou, C. Qin, C. Xu, P. Yan, K. Zhou, J. Hao, X. Yang, Y. Cheng, D.-Y. Wu, Y. Yang, M.-S. Wang, J. Zheng, *Energy Storage Mater.* **2022**, *46*, 406-416.

Author Contributions

P. Bai, X. Ji, Y. Xu and C. Wang conceived the idea of the study. P. Bai conducted the experiments, collected and analyzed the data, and wrote the original draft (lead). Y. Xu and C. Wang supervised the progress and revised the manuscript (equal). J. Zhang and W. Zhang helped formal analysis and discussed the results (supporting). S. Hou helped with the ICP tests (lead). H. Su and M. Li helped formal analysis (supporting). T. Deng helped with XRD tests (lead). L. Cao helped with SEM tests (lead). S. Liu and X. He helped with formal analysis (supporting).